A multi-dimensional, time-lapse, high content screening platform for the flatworm pathogen causing schistosomiasis

Steven Chen[1], Brian M Suzuki[2#], Jakob Dohrmann[3], Rahul Singh[3]*, Michelle R Arkin[1]* & Conor R Caffrey[2#*]

[1]Department of Pharmaceutical Chemistry and Small Molecule Discovery Center, University of California, San Francisco, CA 94143; [2]Center for Discovery and Innovation in Parasitic Diseases, Department of Pathology, University of California, San Francisco, CA 94158; [3]Department of Computer Science, San Francisco State University, San Francisco, CA 94132

[#] Present Address: Center for Discovery and Innovation in Parasitic Diseases, Skaggs School of Pharmacy and Pharmaceutical Sciences, University of California, San Diego, La Jolla, CA 92093

*correspondence to: rahul@sfsu.edu, michelle.arkin@ucsf.edu, ccaffrey@health.ucsd.edu,

Abstract

Approximately ten percent of the world's population is at risk of schistosomiasis, a neglected, parasitic disease of poverty caused by the *Schistosoma* flatworm. To facilitate drug discovery for this complex organism, we developed an automated, time-lapsed high-content (HC) screen to quantify the multi-dimensional responses of *Schistosoma mansoni* post-infective larvae (somules) to chemical insult. We describe an integrated platform to dispense and process worms at scale, collect time-lapsed, bright-field images, segment highly variable and touching worms, and then store, visualize, and interrogate complex and dynamic phenotypes. To demonstrate the method's power, we treat somules with seven drugs that generate diverse responses and evaluate forty-five static and kinetic response descriptors as a function of concentration and time. For compound screening, we use the Mahalanobis distance (d_M) to compare multidimensional phenotypic effects induced by a library of 1,323 approved drugs. We characterize both known anti-schistosomals as well as identify new bioactives. In addition to facilitating drug discovery, the multidimensional quantification provided by this platform will allow mapping of chemistry to phenotype.

Introduction

The *Schistosoma* blood fluke (helminth) causes schistosomiasis, a neglected tropical disease (NTD) [1-3] that infects over 200 million people and puts more than 700 million people at risk of infection in 78 countries [4-6]. Parasite eggs cause chronic inflammatory and fibrotic responses that impair visceral and/or urogenital organ function; co-morbidities include increased risks for bladder cancer and HIV [7, 8]. Praziquantel (PZQ) is the only available drug for schistosomiasis. Although reasonably active against mature schistosomes, PZQ displays little to no efficacy against developing parasites [9, 10]. Also, increased utilization of PZQ raises concerns that drug resistance will emerge. Thus, new drugs are needed [11].

Anthelmintic drug discovery has traditionally relied on phenotypic screens using parasites in culture or in small animal models [12]. Primary screening of cultured schistosomes has often used post-infective larvae (called schistosomula or somules) that can be obtained in their thousands to tens of thousands from vector snails for relatively little effort and cost, in contrast to adult worms that can only be harvested in low numbers (hundreds) from small mammals. Single-metric assays, in which somules are scored as alive or dead, have been reported. (*e.g.*, [13] for review). However, single-metric approaches suffer a number of drawbacks; in some cases, even the clinically used drugs do not score as active in these assays. High-content imaging of live somules offers the potential to visualize complex and non-lethal (but potentially therapeutically relevant) phenotypic responses to drug treatment.

As part of our research program to develop novel methods for anti-schistosomal drug discovery [14-16], we report a fully integrated, automated and multiparametric image-analysis platform for high throughput phenotyping of living parasites. Starting with a set of seven drugs known to induce changes in shape and motion [14, 17], we describe a series of protocols to quantify those changes as a function of time and concentration. We then

demonstrate the utility of the method for high-throughput screening using a set of 1,323 approved drugs. Our approach offers key advances in method integration, including several of general utility to the drug screening/imaging community: a) automated liquid handling of 100 µm-sized organisms, b) manipulation of the focal plane to facilitate identification of low-contrast, variable and touching objects, c) time-lapsed tracking to define frequencies and rates of motion, d) a public system for storage, visualization and querying of the complex phenotypic data, and e) use of a statistical metric (Mahalanobis distance, d_M) to compare multidimensional phenotypes for high-throughput screening.

METHODS

Compounds. K11777 was synthesized via a contract research organization [18]; simvastatin (S1792) was purchased from Selleckchem. PZQ (racemic; P4668), metrifonate (45698) and L-imipramine (I0899, HCl) were purchased from Sigma Aldrich. Sunitinib (S-8803 as the Malate Salt) and staurosporine (S-9300 as the Free Base) were purchased from LC laboratories. The library of approved drugs included 1,129 compounds from the Microsource Drug Collection and an additional 194 compounds donated by Iconix or purchased from commercial vendors. The set included drugs approved by the FDA (85%) and by the analogous European and Japanese agencies (15%).

Somule preparation and plating. The platform design (**Fig. 1**) involves intensive propagation of the molluscan vector to produce 10^4 – 10^5 infective larvae (cercariae) per week sufficient for up to twenty-six 96-well assay plates Cercariae are then mechanically converted [14] into the post-infective schistosomula (somules, ~ 200 x 100 µm) that are relevant to infection in humans.

Each well of a 96-well U-bottom polystyrene assay plate (Corning, Costar 3799) was pre-wetted with 200 µL ddH20 to prevent the formation of bubbles at the well surface. After

aspirating the ddH20, each well received an average of 40 somules in 200 µL Basch medium [19] supplemented with 4% heat-inactivated FBS, 100 U/ml penicillin and 100 mg/ml streptomycin. The somules were suspended in medium using a magnetic tumble stirrer (V&P Scientific, VP 710C1-ALPFX) rotating at 45 rpm, and then dispensed with a 96-channel pipette head (Beckman Coulter Biomek FXp) loaded with sterile 165 µL wide bore filter tips (Axygen, FXF-165-WB-R-S). Eight 96w plates could be prepared per tumbler volume of 200 mL (including a 40 mL dead volume). All assay plates were dispensed in less than 5 min to minimize tumbling damage to the parasite. Compound in neat DMSO was added to the well at the required final assay concentration in 0.1% DMSO using a 96-channel pin tool fitted with 200 nL slotted hydrophobic pins (V&P Scientific, AFIXFX96FP3). Compound was added while shaking the plate at 1,000 rpm in a 0.5 mm radius using a Teleshake 1536 (Variomag) which dispersed the compound from the pin into the surrounding media.

Robotic handling, imaging and analysis. The Momentum 2.0 automation scheduler moved each assay plate from the automated tissue culture incubator (Thermofisher C2, 37^{0}C, 5% CO2) to the barcode reader, then to the automated microscope (GE IN Cell Analyzer 2000), and back to the tissue culture incubator. Each iteration took approximately 35 minutes.

A high-content imager (InCell Analyzer 2000; GE Healthcare) was used to collect 20 seconds of time-lapse images of parasites under one field of view with a 10x objective. The 4 megapixel CCD sensor was binned 4x4 and the bright-field/DAPI channel was set to a 3 ms exposure. The focal plane was offset 40 µm from the bottom of the well to thicken the edge (surface) of the worm. The “sit-and-stare” time-lapse schedule began with a 3.5 second delay to allow time for auto-focusing followed by 30 image acquisitions 0.66 seconds apart.

Images were then analyzed and segmented as described in **Detailed Segmentation Methods**. Features were extracted from the optimal mask chosen from among multiple segmentation attempts for each worm and were stored in a custom MYSQL database for visualization in SchistoView (see Results, **Fig 3**).

RESULTS

High-throughput sample handling for *S. mansoni* somules

We selected somules for primary assays as we can obtain 10^4 – 10^5 somules/week from freshwater vector snails. As somules (~300 x 150 µm) rapidly settle out of solution, we used a magnetic tumble stirrer containing eight stirring paddles to maintain worms in suspension (**Fig. 1**) and allow their transfer using 96- or 384- channel pipets. Plate geometry and number-of-somules/well were optimized for accurate imaging and counting (**Supplementary Fig. 1a**). In particular, U-bottom 96w plates concentrated the parasite as a monolayer into one central field of view, thus facilitating automated imaging. Routine robotic protocols then dispensed compound and shuttled plates between an incubator (Cytomat 2C) and a high-content imager (GE IN Cell Analyzer 2000) for data collection.

Imaging schistosomes by automated, bright-field image analysis

Bright-field, time-lapsed images were generated for control and drug-treated somules using a 10x objective. Every 24 h for 3 days, images were collected at 1.66 Hz (the maximum frame rate for the IN Cell Analyzer 2000) to generate 20 s video recordings. We employed bright-field imaging as it is mechanism-agnostic, non-invasive and fast, and because the schistosome is not yet amenable to the transgenic incorporation of fluorescent proteins. However, in bright-field, somules do not present a high-contrast edge relative to background, thus limiting object segmentation (detection of the object's outline). We, therefore, lowered the focal plane 40 µm below the bottom of the well in

order to artificially generate a dark edge that facilitated segmentation without a significant loss of interior density features (texture; **Supplementary Fig. 1b**).

We observed two strong distributions of somules during our studies. Initially, parasites had a translucent body with a discernable outline. However, under the influence of toxic compounds, worms can become progressively opaque, such that the worm outline is indistinguishable from the interior of the worm. This opacity is associated with degenerating/dying parasites with the transition from "clear" to "opaque" being irreversible. To accurately identify both classes of worms, we segmented the somules using three customized protocols, optimized to detect somules independently by considering the entire worm body, only the worm outline or the worm interior (**Fig. 2**). The largest segmented area obtained from these protocols was selected as the true somule. Each somule was next described using 15 features, including those that defined size, shape, texture and color (for terminology, see **Supplementary Table 1**).

We classified the segmented objects into groups – 'clear' (translucent) worms, 'opaque' (degenerate) worms and 'non-worm' objects. Compared to the clear worm, the average degenerate worm had a lower density level (1,822 ± 49 *vs.* 2,143 +/- 42 levels), lower standard deviation of levels in the mask (227 ± 50 *vs.* 556 ± 49 levels), larger area (6,421 ± 599 *vs.* 3,962 ± 447 μm^2) and a larger form factor (0.66 ± 0.05 *vs.* 0.52 ± 0.06; **Supplementary Table 1**). Combined, these image segmentation protocols identified the somules with a precision of 90% and a recall of 95% when analyzing an average of 40 somules through a timelapse of 30 images (**Supplementary Fig. 1**). In-depth protocols are provided in the **Detailed Segmentation Methods**.

Once worms were classified as clear or degenerate, the 15 calculated features were evaluated across three modes – static, rate and frequency. In the static mode, we considered feature measurements in each frame. In the rate mode, we determined the mean change in a feature between consecutive frames, *e.g.*, rate-of-change in length. In

the frequency mode, we analyzed the number of times the value of a feature increased or decreased, *e.g.*, the number of length contractions/second. As somules showed little translational movement in the u-bottom wells, we did not record their displacement. When combined, the static, rate and frequency modes for each of the 15 features yielded 45 measurements for each somule (see next section).

Two statistical approaches were used to evaluate the significance of changes in worm phenotypes in response to drug treatment. First, the mean and standard deviation for each descriptor for all somules within a well were computed and normalized to determine the Effect Size (ES):

$$ES = \frac{\bar{x} - \mu}{\sigma} \quad \text{(Equation 1)}$$

where $\bar{x}$ is the mean descriptor due to drug exposure, μ is the DMSO mean and σ is the standard deviation of the descriptor for parasites in DMSO [20, 21]. Being dimensionless, ES can be useful in comparing effects across different features where an ES >2 ($p < 0.05$) is generally considered significant. In addition to evaluating individual descriptors, we compared parasites in this descriptor space using the Mahalanobis distance (d_M) [22]. d_M measures the multi-dimensional, scale invariant distance between a test well and a standard condition, *e.g.,* DMSO-treated somules, by taking the result of quadratically multiplying the mean difference and the inverse of the pooled covariance matrix. d_M and ES are similar in that they both measure a distance from the DMSO reference; however, ES measures the distance for just one feature, whereas d_M measures the distance for a group of variables. d_M is not dependent on the measurement unit and can identify test wells that have one large difference or multiple small differences compared to DMSO-treated controls**.**

SchistoView: query-visualization of phenotypic screening data

We developed SchistoView (**Fig. 3,** http://haddock9.sfsu.edu/schistoview/home) which comprises a graphical user interface supported by a MySQL database. SchistoView allows users to visualize and query concentration- and time- dependent somule response data, from computed statistics for a given well to features for individual somules. **Figure 3** shows a screenshot of Schistoview and describes the features of the graphical user interface.

Exploring the parasite's multivariate responses using known anti-schistosomal compounds

We tested the time-lapsed imaging platform with seven compounds that induce diverse changes in the parasite [14, 17]. Somules were exposed to an 11-point, 2.5-fold dilution series (from 2 nM to 20 μM) of compounds in quadruplicate and images were collected after 2, 24 and 48 h. Raw images collected after 24 h of the first frame in each well are shown in **Supplementary Fig. 2**. Images were segmented and data extracted as described above. The results highlight important features of the imaging methodology, the depth of analysis offered and the underlying biology of the schistosome parasite.

The time- and concentration-dependent effects of drugs on worm behavior are visualized using heat maps extracted from SchistoView (**Fig. 4; Supplementary Fig. 3)**. Note that the d_M values shown do not necessarily smoothly change with increasing dose of drug. This is due to individual features showing maximum changes at different concentrations. Using the distribution of d_M as a summary of overall static and kinetic phenotypic change, concentration-dependent effects of drug exposure are already measurable ($p < 0.01$) by 2 h for five of the seven drugs, including PZQ, the kinase inhibitors sunitinib and staurosporine, the anticholinergic imipramine, and the acetylcholine esterase inhibitor (and anti-schistosomal drug) metrifonate. Notably, very little degeneracy is observed at the first time point, except for sunitinib at the two highest

concentrations. After 24 h, d_M remains elevated or increases, and degeneracy becomes apparent for lower concentrations of sunitinib, staurosporine and the HMG-CoA reductase inhibitor, simvastatin. Finally, by 48 h, concentration-dependent degeneracy becomes apparent for five of the compounds with the notable exceptions of PZQ and metrifonate. The absence of cidal activity for these two drugs is consistent with their primary activity as paralytics (see below). Thus, the ability to capture phenotypic changes by d_M [23] (i) affords a rapid and deep assessment of anti-schistosomal activity that is independent of degeneracy and (ii) adds essential value by identifying highly relevant anti-schistosomals that do not induce degeneracy, including the two clinically used drugs, PZQ and metrifonate. Finally, combining static and dynamic descriptors into the d_M provides a more sensitive readout of phenotypic change than either modality alone (**Supplementary Fig. 3**).

The imaging platform quantifies drug-induced increases and decreases in parasite motility. Previously, L-imipramine was visually assessed to induce hypermotility [14]. We confirm this finding and, for the first time, quantify the response. As shown in **Fig. 5a**, imipramine induces a concentration-dependent increase in movement after 2 h between 10 nM and 1 µM (EC_{50} = 100 nM) followed by decreased motility at higher concentrations. This hypermotility is measured as an increasing rate-of-change in length (ES = 1.35; 6 µm/s at ~ 1 µM vs 2 µm/s for DMSO) and increasing frequency (ES = 1; 0.36 Hz at 1 µM vs 0.21 Hz for DMSO). Importantly, the fitted median length never exceeds the minimum or maximum value of DMSO-treated somules at concentrations <8 µM (within ± 0.31 ES); hence, had we just relied on static image-based analysis, imipramine could have been missed as an active compound. By contrast, metrifonate at 2 h (**Fig. 5b**) causes paralysis ($ES_{frequency}$ = -1; 0.09 Hz at 1.3 µM) that is mirrored by an increase in length (ES_{static} = 1.5; 166 µm for 1.3 µM metrifonate *vs.* 137 µm for DMSO). Paralysis is consistent with metrifonate's acetylcholine esterase inhibition [24].

Despite the centrality of PZQ for the treatment of schistosomiasis, its mechanism of action is not well defined and is likely complex, leading to Ca^{++} influx and tetanic paralysis [9]. This complexity is reflected in our phenotypic analysis (**Fig. 5c**). After 2 h, PZQ exhibits a concentration-dependent increase in rate of movement and frequency that peaks at 5 µM (EC_{50} = 389 nM and 196 nM, respectively) that is visualized as 'shivering.' Also, PZQ shows a concentration-dependent shortening of the parasite that reaches a minimum length of 89 ± 3.6 µm at 82 nM (compared to 141 µm for DMSO; ES = -1.7) after which a partial lengthening occurs. The shortening is observed at a 5-fold lower concentration than that needed to increase rate and frequency (EC_{50} = 27 nM for first inflection of the PZQ static-length bell curve and EC_{50} = 147 nM for frequency-length). The difference in concentrations may point to more than one molecular target /mechanism of action for PZQ.

The time-dependence of the shortening effect by PZQ is also different from that of the shivering phenotype. Although both are observed at 2 h (see above), the shortening effect disappears by the 48 h time point (**Supplementary Fig. 4f)**, whereas shivering remains unchanged (**Fig. 3f**). The rapid and small changes in length during shivering are most clearly quantified by frequency (**Fig. 3b**; magenta square at the intersection of length and frequency). These data highlight the *ephemeral* or *transient* nature of some phenotypic responses, a concept that has not yet been considered in anthelmintic screening. Overall, the imaging methodology, as interrogated through SchistoView, allows for the orthogonal identification and quantification of individual concentration- and time-dependent changes.

For the other four members of the seven-drug test set, phenotypic effects at 2 h preceed degeneracy seen at 48 h (**Fig. 4**). For example, two known anti-schistosomal agents, simvastatin [17] and K11777 [18], induce gradual increases in degeneracy (simvastatin EC_{50} = 1 µM at 24 h; K11777 EC_{50} = 20 µM at 48 h). Degeneracy caused by staurosporine is apparent by 24 h and extends across the entire concentration range (**Fig.**

4), consistent with this inhibitor's high affinity for multiple kinases. Other changes include increased area (65% larger than clear worms in DMSO, 13% larger than degenerate worms in DMSO) and increased median diameter (51% larger than clear worms in DMSO, 20% larger than degenerate worms in DMSO; data not shown). Interestingly, within 2 h, sunitinib produces a gray to jet-black phenotype that is much darker than control (DMSO-treated) degenerate worms. The effective concentration for this color change (EC_{50} = 2.94 µM) follows a different concentration-response curve than changes in size, which are elevated at all concentrations. As with PZQ, the complexity of these changes may reflect the time- and concentration-dependent engagement of different targets [25].

Using multi-dimensional features for primary screening

In addition to phenotyping based on inspection of individual descriptors, the experimental platform and SchistoView software are applicable to high-throughput screens using d_M. We prepared 20 x 96-well plates with 40 somules/well that were incubated with DMSO (0.1%) or 10 µM compound from an in-house collection of 1,323 drugs approved for human use. Using the same sample preparation and imaging conditions as for the seven-drug set, plates were robotically handled without manual intervention. Screening proceeded at a maximum rate of one plate/37 min for four scan cycles. Images were automatically processed and analyzed, and data entered into the MySQL database; the screen generated 59,867,820 results for 553,492 segmented worms. The d_M values (calculated from combined static, rate and frequency data), were then extracted and plotted in **Fig. 6a**.

Because d_M does not have an inherent maximum value, the typical screening metric *Z*' cannot be calculated. However, 'hits' are usually picked based on standard deviations from the mean of the negative controls. For the data in **Fig. 6a** (combining static, rate and frequency), a d_M value of 2.47 represents 3 SD from the mean of the DMSO-treated

controls. Using this cutoff value, a total of 237, 263, 326 and 309 hits were identified for cycles 1-4, respectively. Notably, three drugs (PZQ, simvastatin and sunitinib) from the seven-drug test were also present in this screening set, and were identified as active, with d_M value greater than 2.47.

The individual contributions of the static and frequency measurements to the identification of hits were illustrated by calculating a d_M for each measurement in scan cycle 1 (**Fig. 6b**). Of the 216 total hits identified using these individual d_M values, 128 (59%) of the active compounds differed from DMSO-treated worms only in frequency, 32 (15%) compounds differed only by static measurements and 56 (26%) showed a significant response by both static and frequency measures. Overall, when considering rate *vs*. static d_M, the results also point to the importance of motion-based descriptions (**Supplementary Fig. 5**). Thus, 67% of active compounds differed from DMSO-treated worms based on changes in rate but were not significantly different from DMSO based on static features. Hence, quantifying changes in motion was critical to identify the majority of the active compounds in the drug set.

Phenotypes among the 1,323 drug set were remarkably varied. For example, somules exposed to the hormone analog altrenogest displayed static features similar to those of DMSO controls (**Fig. 6b**), but exhibited a 144% increase in frequency of movement by length and a 147% increase in frequency of movement by area. Hence, altrenogest was 'active' based on the d_M for frequency. By contrast, the antifungal, piroctone, only yielded changes in *static* features with a decreased variation in internal texture (63%) and an increase in form factor (110%; yielding a more rounded phenotype) relative to DMSO controls. Somules treated with the adrenergic agonist xylometazoline were altered in both static and dynamic descriptors, *i.e*., a greater mean length of 211 µm *vs.* 130 µm for controls and a 160% increase in frequency of movement by length, respectively.

Consistent with the data in **Fig. 3**, PZQ-treated somules showed a decreased length (82%) and an increased form factor (140%) compared to untreated somules (**Fig. 6b)**.

The data obtained for the 1,323 drug set agree well with results from another drug screen (1,600 drugs tested at 10 µM from the FDA Pharmakon and Microsource Discovery collections) that employed an observation-based scoring system (**Supplementary Table 2**) [26]. Of the 236 compounds for which data were declared in [25], 144 were also screened by us, and for these there was a 67% concordance in the number of actives ($d_{M(static\text{-}rate\text{-}frequency)}$ ≥2.47 (3 SD) and/or degeneracy >50%) and inactives identified. Least agreement occurred for those compounds that yielded significant d_M values but lacked a major degeneracy component, underscoring the added insight of the current fully quantitative approach. Accounting for this group of compounds increased concordance to 72%. Thus, the present screen expands our ability to identify and quantify compounds that induce statistically significant changes in the parasite. Taken together, this new method provides novel and significant features for screening and drug mechanism-of-action: hands-off automation, use of a d_M metric for primary screening and the ability to quantitate complex phenotypic changes

DISCUSSION

The screening platform described here comprises an integrated suite of solutions that solve the bottlenecks hampering drug discovery for global disease pathogens like the schistosome. Issues addressed include: a) producing and dispensing 10^4-10^5 parasites/week to enable automated screening; b) developing a robust image-collection and segmentation protocol and c) designing a system (SchistoView) to store, visualize, query and explore the multivariate data. Using the method, we captured the complexity of the schistosome's response to seven drugs and identified novel screening hits from a drug library. The data highlight the importance of quantifying changes in motion on the

seconds timescale. This scale and quantitative depth have not been achieved before for schistosomes or other parasitic helminths and the method is, in principle, adaptable to other organisms.

Somules are difficult to image due to their (variability in) movement and because they have a low contrast in bright field. We solved the image-collection challenge using round-bottom wells to constrain worms into one visual field and thus limit translation. We then addressed their low contrast by focusing slightly below the worm to enhance its outline. From there, we observed two basic classes of worms – clear and opaque – and optimized segmentation protocols for each. The resulting segmentation accuracy (precision of 90% and a recall of 95%, **Supplementary Fig 1a**) is an improvement on a previous report that employed bright field analysis (24.5±7%) where touching somules could not be evaluated [27]. Also, our imaging approach economizes on the number of parasites needed by 3-4 fold and measures *how* worms move rather than a simple classification of whether movement has occurred [27]. Finally, our methodology provides a solution to the critical issue of segmentation of touching objects in the analysis of bright field images generally [28-30].

The live imaging platform described here can be incorporated into a drug discovery pipeline upstream of *ex vivo* phenotypic screens of the adult schistosomes and rodent models of infection[14]. Recent advances in the image-based quantification of adult schistosome motility[31, 32] have demonstrated the ability to quantify motion and could mesh seamlessly with the workflow described here. The platform will complement other advances relating to schistosome biology, including gene expression profiling [33], metabolomics [34], and CRISPR/Cas9 [35], that together will improve our ability to holistically quantify this globally important parasite's response to a range of drug-induced, environmental and developmental phenotypes. To facilitate such discoveries, the database and SchistoView interface are available online.

ACKNOWLEDGEMENTS: We thank the following funding sources: NIH AI146719, NIH AI089896, and NSF IIS-1817239.

AUTHOR CONTRIBUTIONS: C.R.C, B.M.S. and S.C. performed the screens. S.C. designed the scripts for image analysis. S.C. and J.D. built the code for SchistoView and all authors contributed to its design. All authors interpreted the data and contributed to the manuscript.

FIGURES

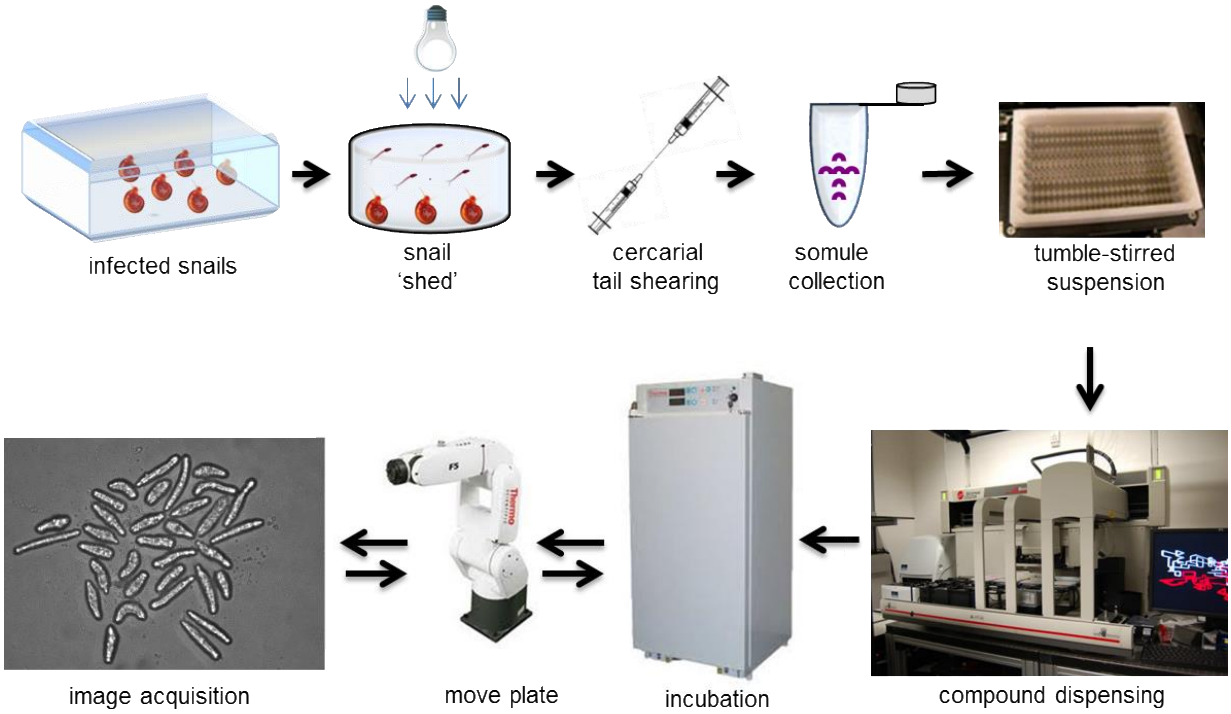

Figure 1. Assay workflow. Infected *Biomphalaria glabrata* vector snails were stimulated under light to release ('shed') 10^4–10^5 *Schistosoma mansoni* infective larvae (cercariae) per week. Cercariae were mechanically converted to post-infective larvae (schistosomula or somules) using a 20-gauge double-headed syringe needle. After washing to remove cercarial tails, somules were suspended in a paddle-stirred reservoir. Somules were dispensed into 96-well u-bottom clear plates at 40 units/well/200 µL Basch medium. Compounds were added using a 96-channel pin tool. Plates were maintained at 5% CO_2 and 37 °C. At specified time points, a 6-axis robotic arm transferred the plates to the high-content imager.

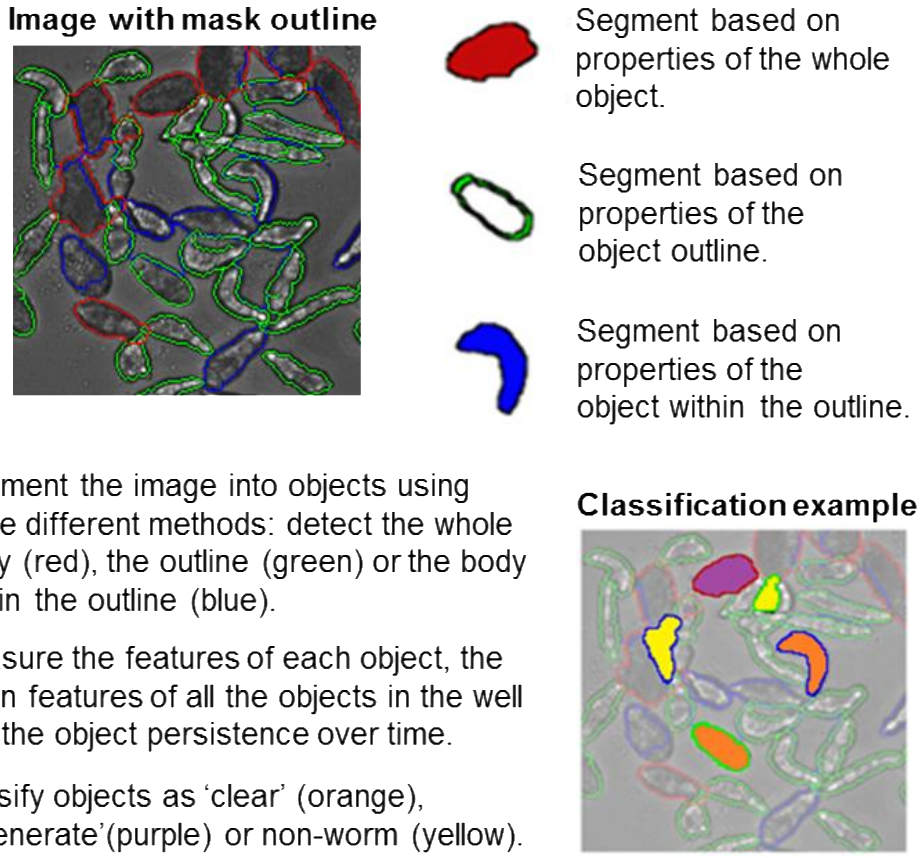

Figure 2. Summary of segmentation and data post-process workflow. Details provided in the **Detailed Segmentation Methods**. Acquired images (30 time-lapse images per well) were loaded into the IN Cell Developer software and segemented. 'Clear' worms, 'opaque' worms and non-worm objects were classified based on features computed for 20,000 worm and non-worm objects.

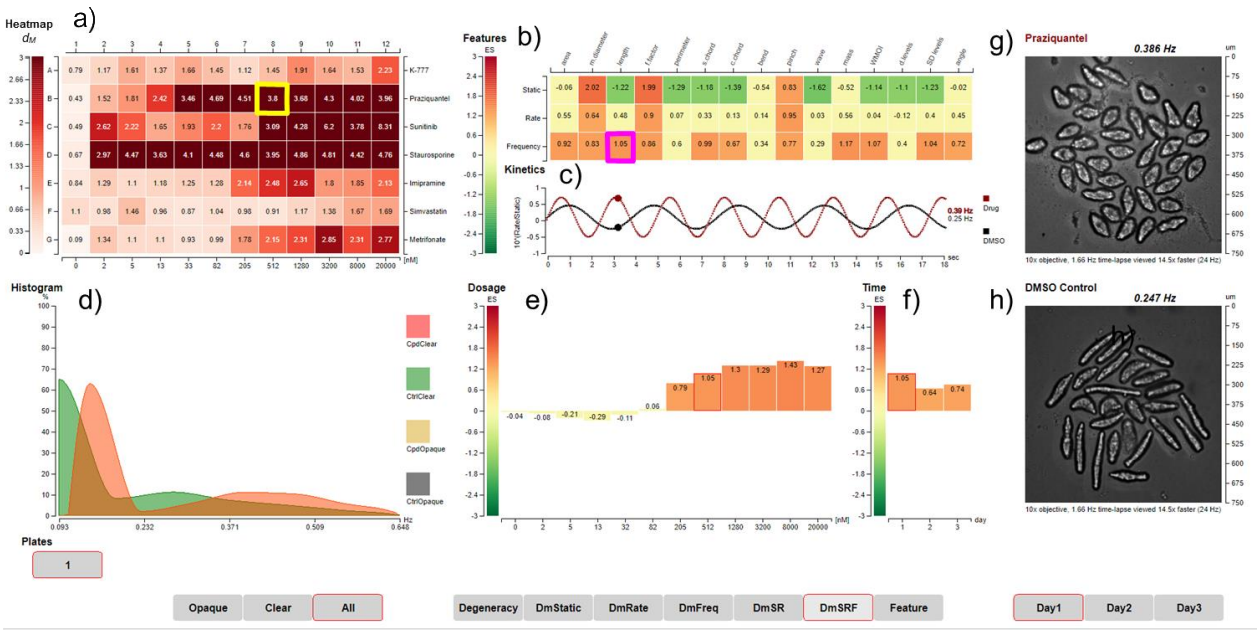

Figure 3. Screenshot of the SchistoView graphical user interface. Selected data at the 2 h timepoint are shown to illustrate the hierarchical approach to visualization. (**a**) Heat map of Mahalanobis distances (d_M) for seven test drugs arrayed over an 11-point, 2.5-fold dilution series (from 2 nM in column 2 to 20 µM in column 12). From top to bottom, the drugs are K11777, PZQ, sunitinib, staurosporine, imipramine, simvastatin and metrifonate. DMSO controls are arrayed in column 1. The average d_M for each DMSO control is shown. A d_M of 1.61 is significantly different from control ($p < 0.01$). Clicking on well B8 of the heat map (representing 512 nM PZQ and identified by the yellow square) populates panels (**b**) through (**g**) in the GUI. (**b**) Heat map showing the effect sizes (ES) for each of 15 features (columns) plotted as a function of static, rate or frequency modes (rows); a 'descriptor' is the combination of a given feature and mode. Clicking on a descriptor, *e.g.*, frequency of change in length (identified by the magenta square) populates panels (**c**) – (**f**). (**c**) Calculated waveforms defined by the mean length (baseline), range of length (amplitude) and frequency of length contraction (frequency). DMSO control worms (black line) are longer (higher baseline) and slower moving (lower

frequency) than those treated with 512 nM PZQ at 2 h (red line). (**d**) Histogram displaying the distribution of frequency of length contraction for DMSO control worms (green) and PZQ-treated worms (orange). **(e)** Bar graph depicting the ES for the frequency of length contraction after 2 h of PZQ treatment across the 11 tested concentrations. (**f**) Bar graph depicting the ES for the frequency of length contraction in the 512 nM PZQ treatment across the three days indicated. (**g**) First image from time-lapsed movie of well B8 highlighted in (**a**); in the live SchistoView, the 30-frame movie is shown. (**h**) First image from time-lapsed movie of a DMSO-treated well; in the live SchistoView, the 30-frame movie is shown. Buttons along the bottom of the figure are used in SchistoView to select the plate (1), the somules analyzed (Opaque, Clear, All), the mode displayed in panel (**a**) (*i.e.,* degeneracy; d_M for static features, d_M for rate, d_M for frequency; d_M for static and rate; d_M for static, rate and frequency or a single feature), and the day of the experiment (Day 1, 2 or 3).

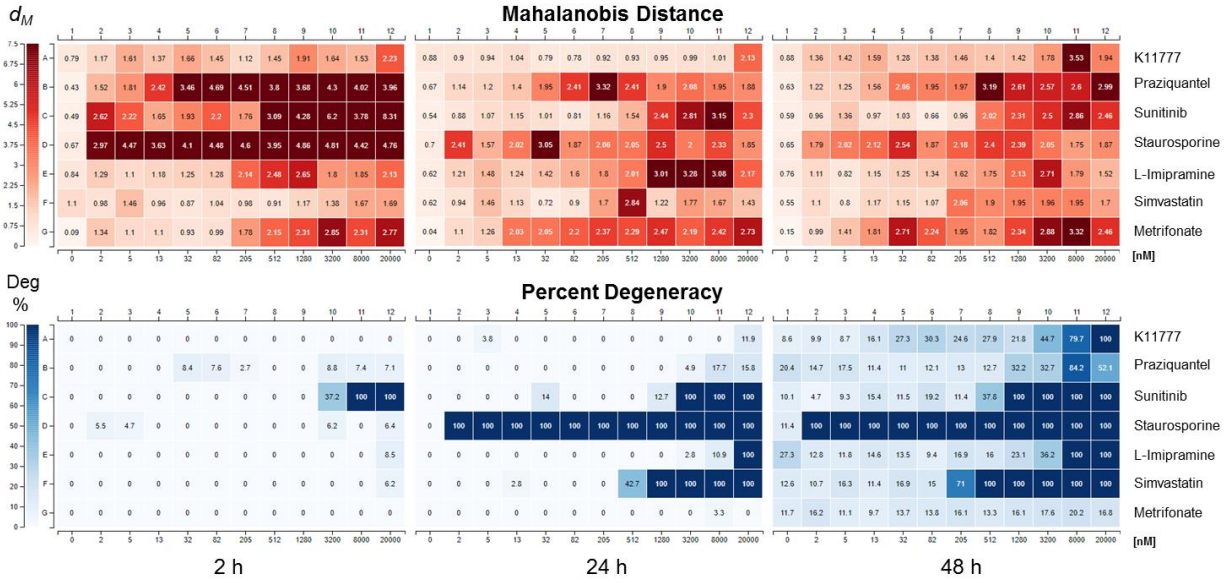

Figure 4. Heat map displaying d_M and degeneracy for seven test drugs arrayed over a 2.5-fold dilution series from 20 μM to 2 nM. d_M values were calculated relative to DMSO controls (not shown). A d_M value of 1.61, 1.36 and 1.28 is significantly different from control ($p < 0.01$) for 2, 24 and 48 h, respectively. Results presented are aggregated from four wells per treatment group (40 somules/well). For most compounds, phenotypes appear quickly (within 2 or 24 h), relative to the appearance of degeneracy (pronounced at 48 h). Notably, the two approved anti-schistosomal drugs, PZQ and metrifonate, do not induce significant degeneracy under these conditions. The d_M values shown do not necessarily smoothly change with increasing dose of drug. This complexity reflects the observation that multiple parameters show maximum changes at different doses.

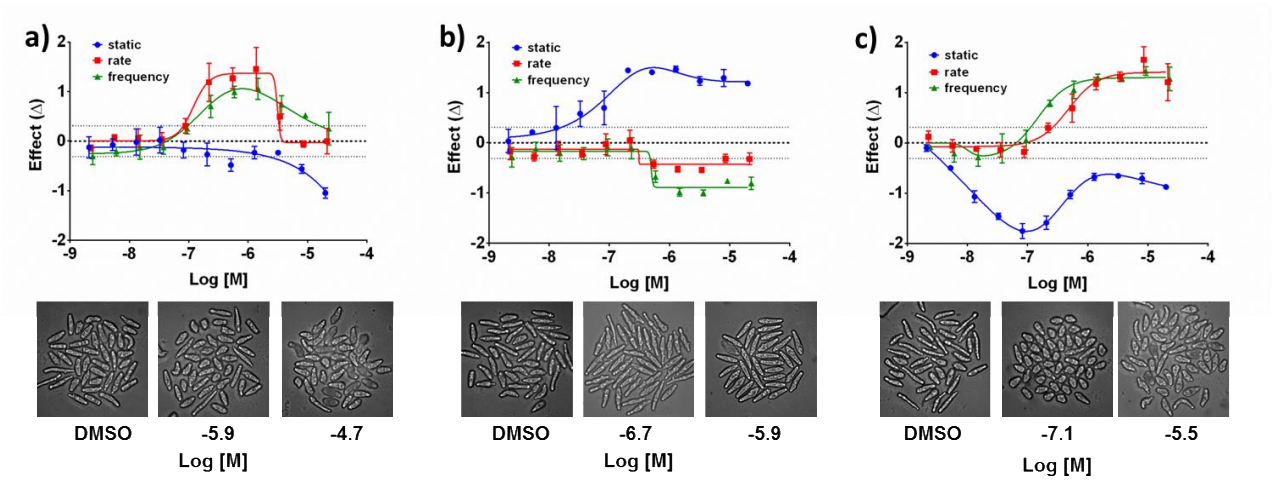

Figure 5. Concentration-dependent phenotypic responses to anti-schistosomal drugs after 2 h. Compound concentrations (2 nM – 20 μM) are plotted *vs*. effect size (ES). The graphs display changes in mean length (blue), rate-of-change of length (red) and frequency of changes in length/contractions (green) for (**a**) L-imipramine, (**b**) metrifonate and (**c**) PZQ. Error bars represent the standard deviation from four replicate wells at each concentration. Images of the somules at selected drug concentrations are shown below each graph.

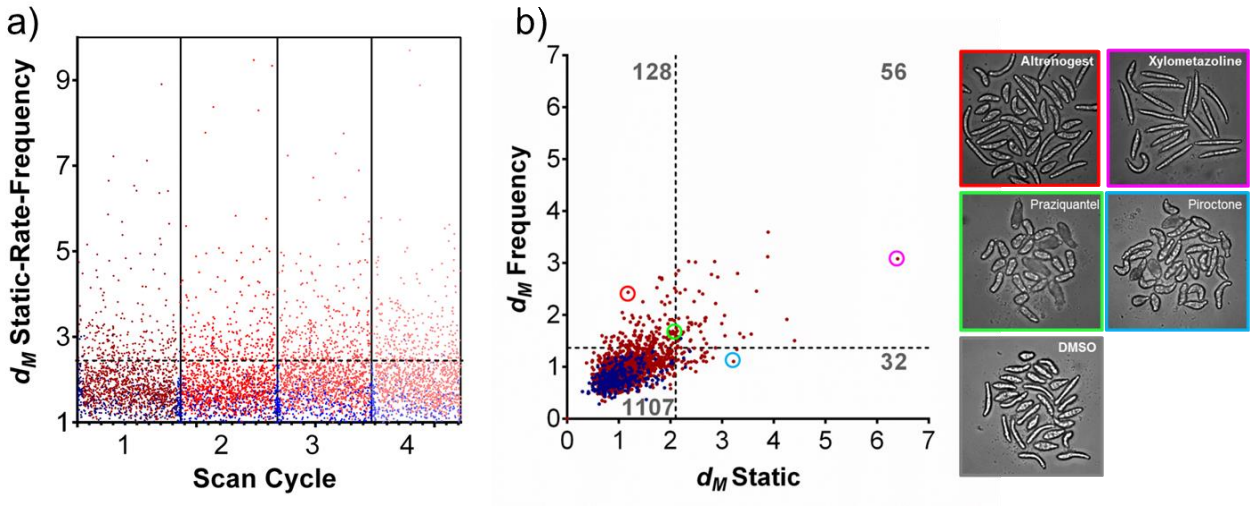

Figure 6. Scatterplot of data from a primary screen of 1,323 approved drugs. (**a**) Twenty plates were imaged over four scan cycles, each representing approximate intervals of 24 h. DMSO controls are shown in blue and the tested drugs (10 µM) are in red. d_M values take into account static, rate and frequency modes. The horizontal dashed line represents the d_M value (2.47) that is 3 SD from the mean of the DMSO controls. The number of drugs with $d_M \geq 2.47$ are 237, 263, 326 and 309 compounds for scan cycles 1 through 4, respectively. (**b**) Scatter plot showing contributions of d_M based on static (x-axis) *vs.* frequency (y-axis) modes for the first scan cycle. The dashed lines represent the d_M values that are 3 SD from the DMSO mean (2.1 for $d_{M(static)}$ and 1.4 for $d_{M(frequency)}$). The number of drugs in each quadrant is indicated in grey font: 1,107 drugs were inactive; 32 drugs induced static phenotypes only, 128 induced only kinetic phenotypes and 56 compounds induced significant changes in both modes. The frames of the images to the right are color-matched with the highlighted compounds in the plot: note the remarkable range of phenotypes presented by this parasite.

REFERENCES

1. Warren, K.S., *Hepatosplenic schistosomiasis: a great neglected disease of the liver.* Gut, 1978. **19**(6): p. 572-7.
2. Hotez, P.J., et al., *The global burden of disease study 2010: interpretation and implications for the neglected tropical diseases.* PLoS Negl Trop Dis, 2014. **8**(7): p. e2865 DOI: 10.1371/journal.pntd.0002865.
3. Hotez, P.J., A. Damania, and M. Naghavi, *Blue Marble Health and the Global Burden of Disease Study 2013.* PLoS Negl Trop Dis, 2016. **10**(10): p. e0004744 DOI: 10.1371/journal.pntd.0004744.
4. King, C.H., *Parasites and poverty: the case of schistosomiasis.* Acta Trop, 2010. **113**(2): p. 95-104.
5. Steinmann, P., et al., *Schistosomiasis and water resources development: systematic review, meta-analysis, and estimates of people at risk.* Lancet Infect Dis, 2006. **6**(7): p. 411-25.
6. WHO, *Schistosomiasis and soil-transmitted helminthiases: numbers of people treated in 2017.* Weekly Epidemiological Record, 2018. **50**(93): p. 681–692.
7. Colley, D.G., et al., *Human schistosomiasis.* Lancet, 2014. **383**(9936): p. 2253-64 DOI: 10.1016/S0140-6736(13)61949-2.
8. Galappaththi-Arachchige, H.N., et al., *Reproductive health problems in rural South African young women: risk behaviour and risk factors.* Reprod Health, 2018. **15**(1): p. 138 DOI: 10.1186/s12978-018-0581-9.
9. Andrews, P., et al., *Praziquantel.* Med Res Rev, 1983. **3**(2): p. 147-200.
10. Sabah, A.A., et al., *Schistosoma mansoni: chemotherapy of infections of different ages.* Exp Parasitol, 1986. **61**(3): p. 294-303.
11. Caffrey, C.R., *Schistosomiasis and its treatment.* Future Med Chem, 2015. **7**(6): p. 675-6 DOI: 10.4155/fmc.15.27.
12. Geary, T.G., J.A. Sakanari, and C.R. Caffrey, *Anthelmintic drug discovery: into the future.* Journal of Parasitology, 2015. **101**(2): p. 125-133 DOI: 10.1645/14-703.1.
13. Panic, G., et al., *Fluorescence/luminescence-based markers for the assessment of Schistosoma mansoni schistosomula drug assays.* Parasit Vectors, 2015. **8**: p. 624 DOI: 10.1186/s13071-015-1233-3.
14. Abdulla, M.H., et al., *Drug discovery for schistosomiasis: hit and lead compounds identified in a library of known drugs by medium-throughput phenotypic screening.* PLoS Negl Trop Dis, 2009. **3**(7): p. e478 DOI: 10.1371/journal.pntd.0000478.
15. Asarnow, D., et al., *The QDREC web server: determining dose-response characteristics of complex macroparasites in phenotypic drug screens.* Bioinformatics, 2015. **31**(9): p. 1515-8 DOI: 10.1093/bioinformatics/btu831.
16. Singh, R., et al., *Algorithmic Mapping and Characterization of the Drug-Induced Phenotypic-Response Space of Parasites Causing Schistosomiasis.* IEEE/ACM Trans Comput Biol Bioinform, 2018. **15**(2): p. 469-481 DOI: 10.1109/TCBB.2016.2550444.
17. Rojo-Arreola, L., et al., *Chemical and genetic validation of the statin drug target to treat the helminth disease, schistosomiasis.* PLoS ONE, 2014. **9**(1): p. e87594 DOI: 10.1371/journal.pone.0087594.
18. Abdulla, M.H., et al., *Schistosomiasis mansoni: novel chemotherapy using a cysteine protease inhibitor.* PLoS Med, 2007. **4**(1): p. e14.
19. Basch, P.F., *Cultivation of Schistosoma mansoni in vitro. I. Establishment of cultures from cercariae and development until pairing.* J Parasitol, 1981. **67**(2): p. 179-85.

20. Nakagawa, S. and I.C. Cuthill, *Effect size, confidence interval and statistical significance: a practical guide for biologists.* Biol Rev Camb Philos Soc, 2007. **82**(4): p. 591-605 DOI: 10.1111/j.1469-185X.2007.00027.x.
21. Hedges, L. and I. Olkin, *Statistical Methods for Meta-Analysis.* . 1985, Orlando: Academic Press.
22. Mahalanobis, P.C., *On the generalized distance in statistics.* Proceedings of the National Institute of Sciences (India), 1936. **2**(1): p. 49-55.
23. Reisen, F., et al., *Benchmarking of multivariate similarity measures for high-content screening fingerprints in phenotypic drug discovery.* J Biomol Screen, 2013. **18**(10): p. 1284-97 DOI: 10.1177/1087057113501390.
24. Camacho, M., et al., *The amount of acetylcholinesterase on the parasite surface reflects the differential sensitivity of schistosome species to metrifonate.* Parasitology, 1994. **108 (Pt 2)**: p. 153-60.
25. Karaman, M.W., et al., *A quantitative analysis of kinase inhibitor selectivity.* Nat Biotechnol, 2008. **26**(1): p. 127-32 DOI: 10.1038/nbt1358.
26. Panic, G., et al., *Activity Profile of an FDA-Approved Compound Library against Schistosoma mansoni.* PLOS Neglected Tropical Diseases, 2015. **9**(7): p. e0003962 DOI: 10.1371/journal.pntd.0003962.
27. Paveley, R.A., et al., *Whole organism high-content screening by label-free, image-based Bayesian classification for parasitic diseases.* PLoS Negl Trop Dis, 2012. **6**(7): p. e1762 DOI: 10.1371/journal.pntd.0001762.
28. Chalfoun, J., et al., *FogBank: a single cell segmentation across multiple cell lines and image modalities.* BMC Bioinformatics, 2014. **15**: p. 431 DOI: 10.1186/s12859-014-0431-x.
29. Qi, X., et al., *A fast, automatic segmentation algorithm for locating and delineating touching cell boundaries in imaged histopathology.* Methods Inf Med, 2012. **51**(3): p. 260-7 DOI: 10.3414/ME11-02-0015.
30. Selinummi, J., et al., *Bright field microscopy as an alternative to whole cell fluorescence in automated analysis of macrophage images.* PLoS One, 2009. **4**(10): p. e7497 DOI: 10.1371/journal.pone.0007497.
31. Marcellino, C., et al., *WormAssay: a novel computer application for whole-plate motion-based screening of macroscopic parasites.* PLoS Negl Trop Dis, 2012. **6**(1): p. e1494 DOI: 10.1371/journal.pntd.0001494.
32. Melo-Filho, C.C., et al., *QSAR-Driven Discovery of Novel Chemical Scaffolds Active against Schistosoma mansoni.* J Chem Inf Model, 2016. **56**(7): p. 1357-72 DOI: 10.1021/acs.jcim.6b00055.
33. Picard, M.A., et al., *Sex-biased transcriptome of Schistosoma mansoni: host-parasite interaction, genetic determinants and epigenetic regulators are associated with sexual differentiation.* PLoS Negl Trop Dis, 2016. **10**(9): p. e0004930 DOI: 10.1371/journal.pntd.0004930.
34. Preidis, G.A. and P.J. Hotez, *The newest "omics"--metagenomics and metabolomics--enter the battle against the neglected tropical diseases.* PLoS Negl Trop Dis, 2015. **9**(2): p. e0003382 DOI: 10.1371/journal.pntd.0003382.
35. Ittiprasert, W., et al., *Programmed genome editing of the omega-1 ribonuclease of the blood fluke, Schistosoma mansoni.* Elife, 2019. **8** DOI: 10.7554/eLife.41337.

Supplementary Figures and Tables

Supplementary Table 1. Glossary of Terms.

Term	Description	Units
Area	Area of a target	μm^2
Median Diameter	The median internal distance perpendicular to the maximum curved chord.	μm
Length	Maximum distance across a target. Boundaries may be crossed.	μm
Form Factor	Estimate of circularity, expressed as a value between 0 and 1 (1 equals a perfect circle).	value
Perimeter	Distance around a target.	μm
Straight Chord	The maximum straight-line distance across a target without crossing a boundary.	μm
Curved Chord	Maximum center line through target.	μm
Bend	Bend = (max curved chord / max straight chord).	ratio
Pinch	Pinch = (median diameter * length) / area) is the estimated area divided by the actual area.	ratio
Wave	Wave = Perimeter / (2 * Area^$^{0.5}$) is the actual perimeter divided by the estimated perimeter.	ratio
Mass	The sum of all pixel values in the shape.	sum
WMOI	(Weighted Moment of Inertia) Index of the homogeneity of gray levels within a circular target. A value of 1 indicates the target is relatively homogeneous. If >1, the target has a higher proportion of bright pixels in its center. If <1, the target has a higher proportion of bright pixels around its perimeter.	index
Density - Levels	Mean gray level value of the pixels contained within the target outline. Gray levels is an intensity scale, where black = 0 and white = 4095 (12-bit image).	Levels
SD - Levels	A standard deviation (SD) of pixel densities, which measures the pixel density variation within the target. SD values are available for any density unit.	levels
Angle	Angle of the straight chord relative to the horizontal (horizontal = 0 degrees). Negative values are clockwise from horizontal; positive values are counter-clockwise.	degrees
Rate	The average amount of changes between sequential time-lapse images.	“units”/frame
Frequency	The number of times a feature changes direction.	Hz
Effect Size (ES)	ES = (x-μ)/σ where x is the drug mean, μ is the DMSO mean, and σ is the standard deviation of DMSO. No unit, but the magnitude of the measurement can be thought of as the number of standard deviations from the DMSO control group for the selected feature.	
Mahalanobis Distance (d_M)	d_M is a multi-dimensional effect size which measures the distance of a test point from a reference distribution. No unit, but the magnitude of the measurement can be thought of as the number of standard deviations from the DMSO control group.	

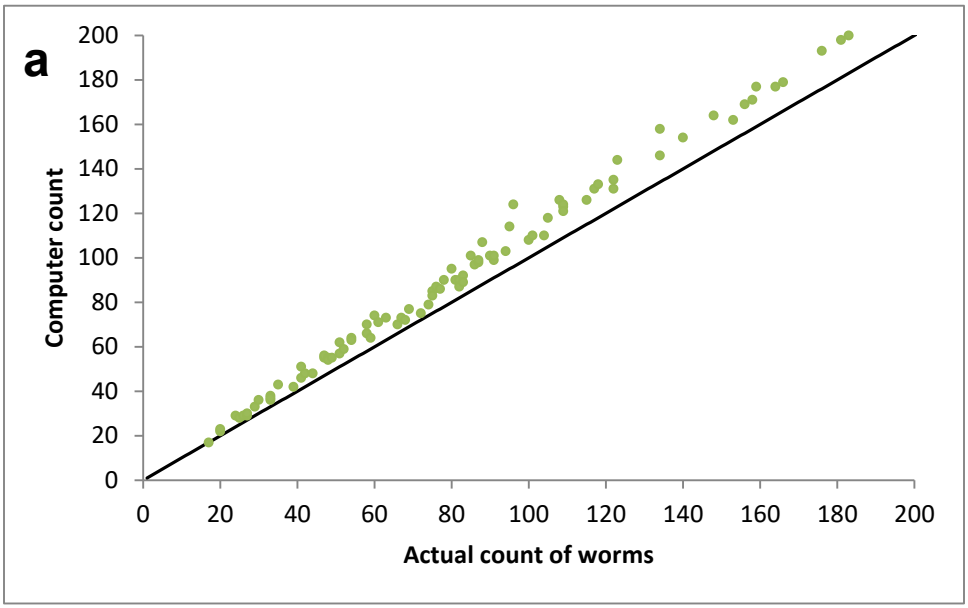

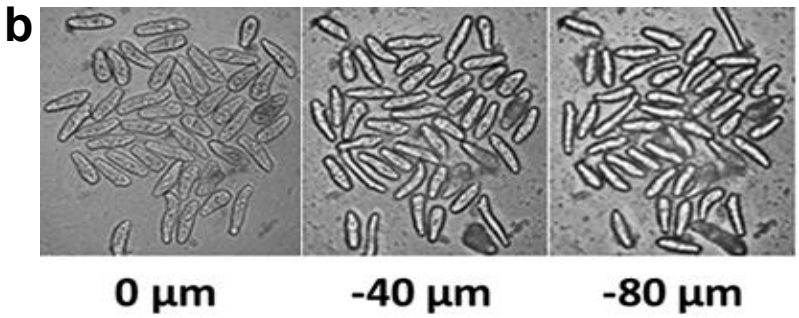

Supplementary Figure 1. Optimizing parasite handling and segmentation. **(a)** Comparison of actual worms (counted by visual inspection) and the number of worm objects identified by the object classifier algorithm 'computer count'. Computational inclusion of non-worm objects with worm-like features leads to a systematic 10% increase in object count. **(b)** Images from a single sample well imaged at three focal planes (0, -40, and -80 µm from the outside bottom of the well). Lowering the focal plane improves the contrast of the somule outline ('edge'). Minus 40 microns improves the appearance of the outline while preserving some of the internal texture detail.

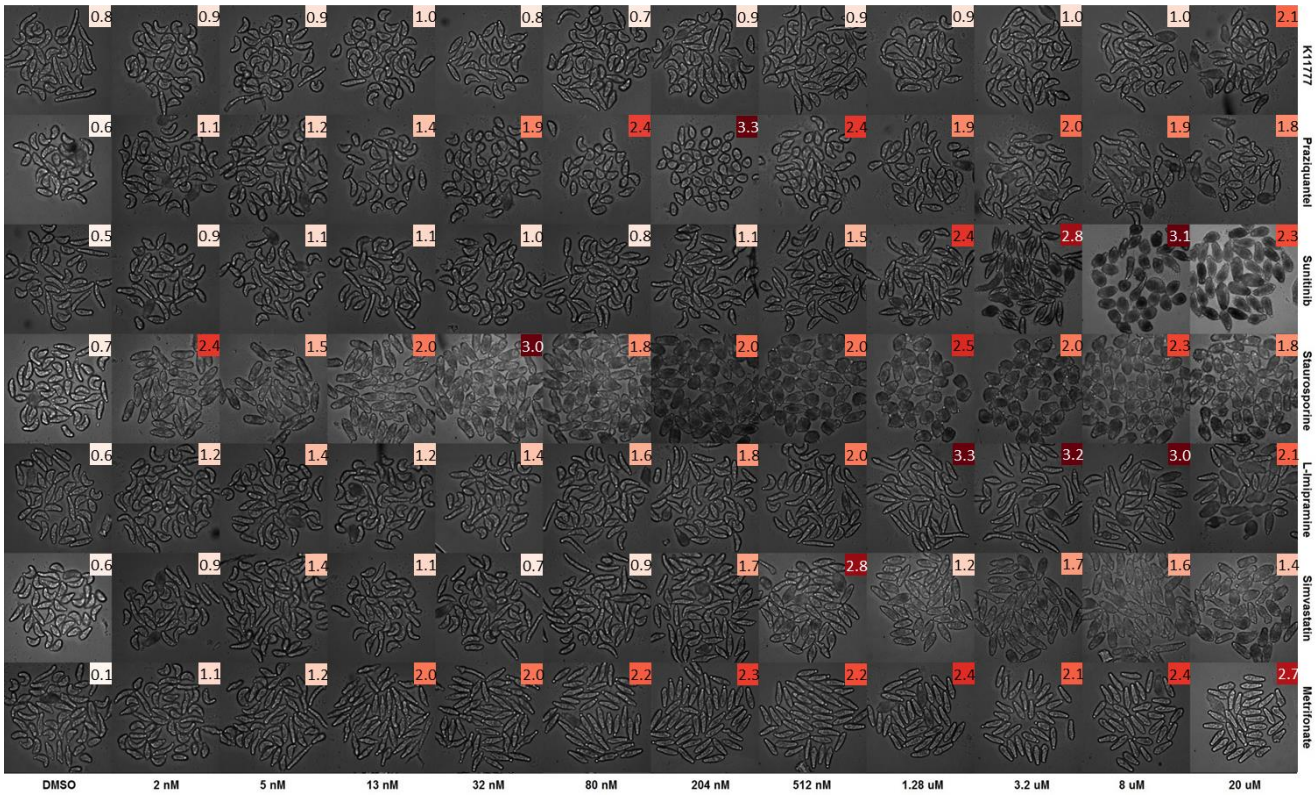

Supplementary Figure 2. Montage of somule images 24 h after treatment with seven test drugs. Drug names are to the right; concentrations are at the bottom. Each image in the montage is labeled with the corresponding d_M value and scaled color.

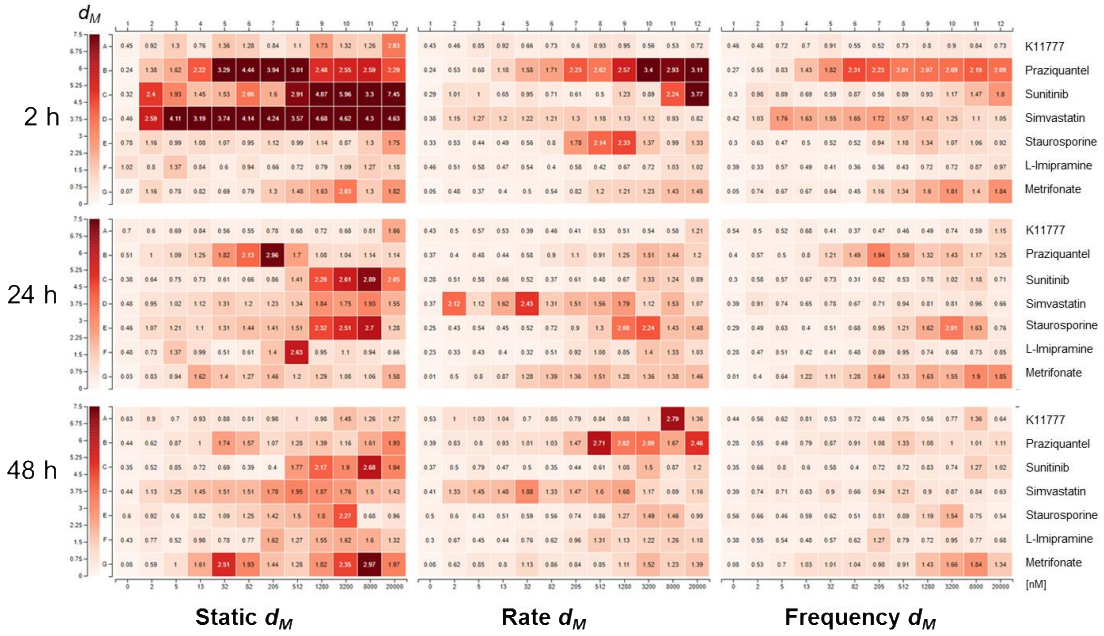

Supplementary Figure 3. Differing sensitivities of static $d_{M,}$ rate $d_{M,}$ and frequency d_M to measuring drug effects. Mahalanobis distances (d_M) 2, 24 or 48 h after treatment and measured using only static features (left panels), rate (center panels) or frequency for seven test drugs. Drugs were arrayed over an 11-point 2.5-fold dilution range from 2 nM to 20 µM. Scores were derived from the aggregation of four wells per treatment. Note that the d_M values shown do not necessarily smoothly change with increasing dose of drug. This complexity reflects the observation that multiple parameters show maximum changes at different concentrations. Note the added value brought by the ability to measure more than one mode, *e.g.*, $d_{M(static\ +\ frequency)}$ vs. $d_{M(rate)}$ for 32 – 512 nM praziquantel at 24 h; or $d_{M(rate)}$ for 205 – 1280 nM imipramine vs. $d_{M(static\ +\ frequency)}$ at 2 h.

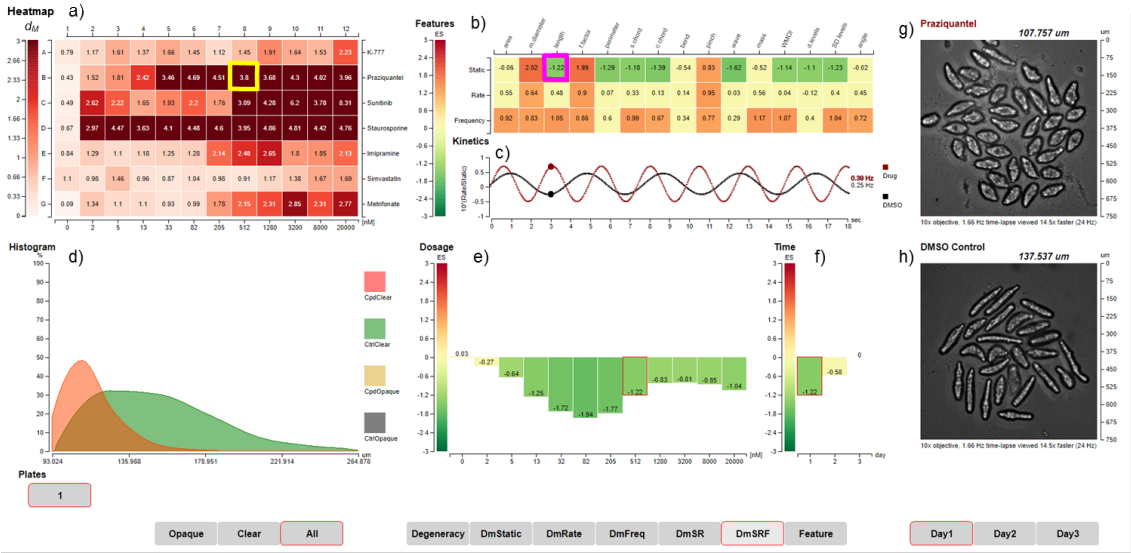

Supplementary Figure 4. Screenshot of the SchistoView graphical user interface. The figure is analogous to **Fig 3**, but highlights the length of PZQ-treated somules whereas **Fig 3** shows the frequency of changes in length. Selected data are shown to illustrate the hierarchical approach to visualization. **(a)** Heat map of Mahalanobis distances (d_M) for seven test drugs arrayed over an 11-point 2.5-fold dilution series from 2 nM in column 2 to 20 µM in column 12. Drugs, from top to bottom, are, K11777, PZQ, sunitinib, staurosporine, imipramine, simvastatin and metrifonate. DMSO controls are arrayed in column 1 and are shown as the average d_M (0.77) for all DMSO controls. A d_M of 1.61 is significantly different from control ($p < 0.01$). Clicking on coordinate B8 (identified by the yellow square: 512 nM PZQ) populates panels (**b**) and (**g**) (see below). **(b)** Heat map showing the effect sizes (ES) for static, rate and frequency, after exposure to 512 nM PZQ for 2 h, *i.e.*, the selected well from (**a**). Three sets of 15 features are arrayed in rows and columns, respectively. Clicking on the intersection of the length feature and static mode (magenta box) in (**b**) populates panels (**c**) through (**f**) and the underlying data. (**c**) Calculated waveforms defined by the range of length (amplitude) and frequency of length contraction (frequency). DMSO control worms are slower moving (lower frequency) than those treated with 512 nM PZQ (red line). (**d**) Histogram displaying the distribution of frequency of length contraction for DMSO control worms (green) and PZQ-treated worms (orange). (**e**) Bar graph depicting the ES for the frequency of length contraction after PZQ treatment across 11 concentrations (second row in (**a**)). (**f**) Bar graph depicting the ES for the frequency of length contraction in the 512 nM PZQ treatment across the three days of measurement. **(g)** First image from time-lapsed movie of the well highlighted in **a**; in the live SchistoView, the 30-frame movie is looped. (**h**) as for (**g**) except for the DMSO control.

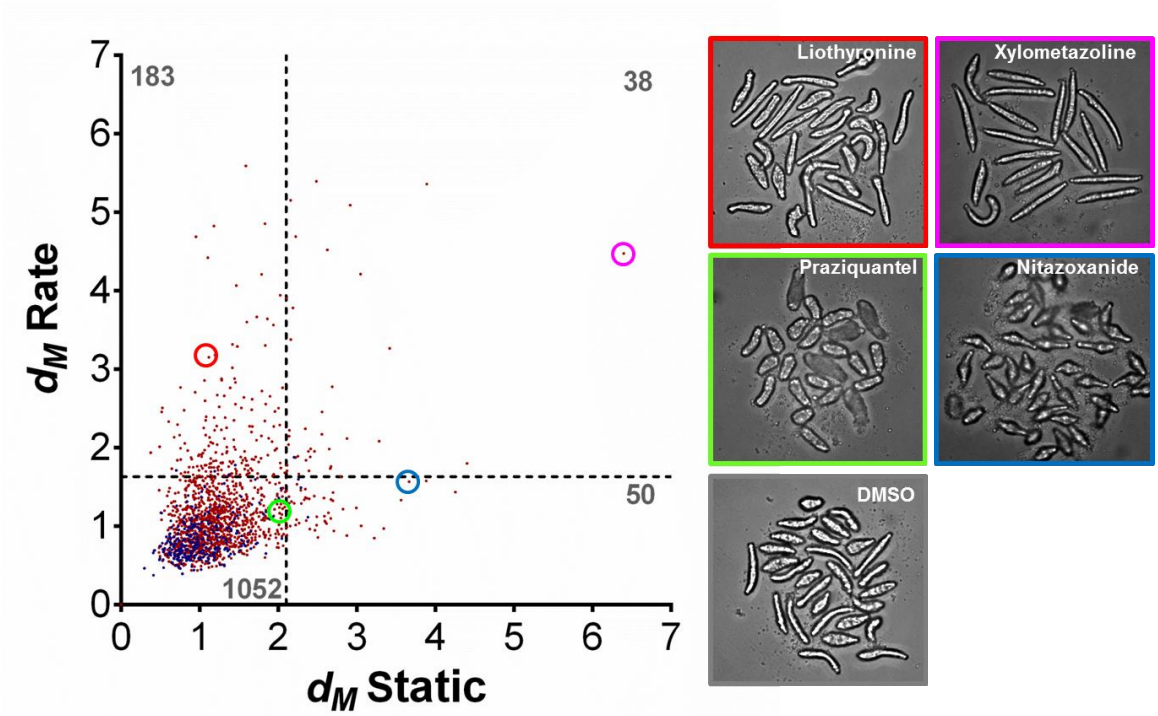

Supplementary Figure 5. Scatterplot of $d_{M(rate)}$ *vs*. $d_{M(static)}$ for a primary screen of 1,323 approved drugs. Like **Fig 6b** in the main text, which shows a scatterplot of $d_{M(frequency)}$ *vs*. $d_{M(static)}$, the screen was performed at 10 µM. The data shown are from the first scan cycle approximately 24 h after the addition of drug. The dashed lines represent the d_M values that are 3 SD from the DMSO mean (2.1 for $d_{M(static)}$ and 1.6 for $d_{M(rate)}$). The number of drugs in each quadrant is indicated in dark grey for both static and rate modes: 1,052 drugs were inactive, 50 drugs induced static phenotypes only, 183 induced only kinetic phenotypes and 38 compounds induced significant changes in both modes. The frames of the images to the right are color-matched with the highlighted compounds in the plot: note the remarkable range of phenotypes presented by this parasite.